Beam-Waveguide Antenna Performance Predictions with Comparisons to Experimental Results

Dan A. Bathker, *Senior Member, IEEE,* Watt Veruttipong, *Senior Member, IEEE,* Tom Y. Otoshi, *Senior Member, IEEE,* and Paul W. Cramer, Jr.

***Abstract*—This article presents an overview of a NASA/JPL antenna project, with specific focus on the methodology used to predict the microwave performance of a new 34-m-diameter beam-waveguide (BWG) reflector antenna, designated DSS 13. Deep Space Station 13 is the research and development facility serving the NASA/JPL Deep Space Network. Three companion articles in this issue detail the microwave test packages, test results, and microwave holography-based evaluations and alignment. This article provides microwave performance predictions as well as a summary of test results for the antenna, which has Cassegrain and centerline BWG operating modes at *X*-band (8.450-GHz) and *Ka*-band (32-GHz) frequencies. Predictions were used to identify critical and poorly understood areas needing further study and diagnostic testing, and assisted in planning, scheduling, and evaluating the final results of a detailed test program. Predictions were assembled for all known losses that contribute to antenna performance degradations, including antenna area efficiencies, corresponding beampeak gains, and noise temperatures. It was found that predictions and experimental results agreed reasonably well for beampeak gain and corresponding efficiency, and for several (but not all) noise temperatures. It is believed that the performance predictions and measurements described herein may be the most detailed and accurate available for a large reflector antenna with two significant operating modes and two frequencies.**

I. Introduction

A NEW 34-m-diameter beam-waveguide (BWG) antenna has been built at the NASA/JPL Deep Space Station 13 (DSS 13) in the Goldstone Deep Space Communications Complex near Barstow, CA. The new antenna is the first NASA tracking antenna to use a BWG design. Fig. 1 shows a front view of the new BWG antenna pointed in the zenith direction depicting the subreflector, subreflector tripod supports, and some of the solid and perforated panel sections of the main reflector. Fig. 2 is a line drawing of the rear view of the new antenna depicting the main BWG centerline mode with focal points f1 and f3. Focal point f1 is the normal (Cassegrain) focus located close to the vertex of the main reflector, while focal point f3 is about 35 m and six additional reflectors distant, in a subterranean room. Focal point f2 is not normally used. For simplification, a completely independent (bypass) BWG for other purposes, visible in Figs. 1 and 2 with yet a fourth focal point, is not further discussed herein.

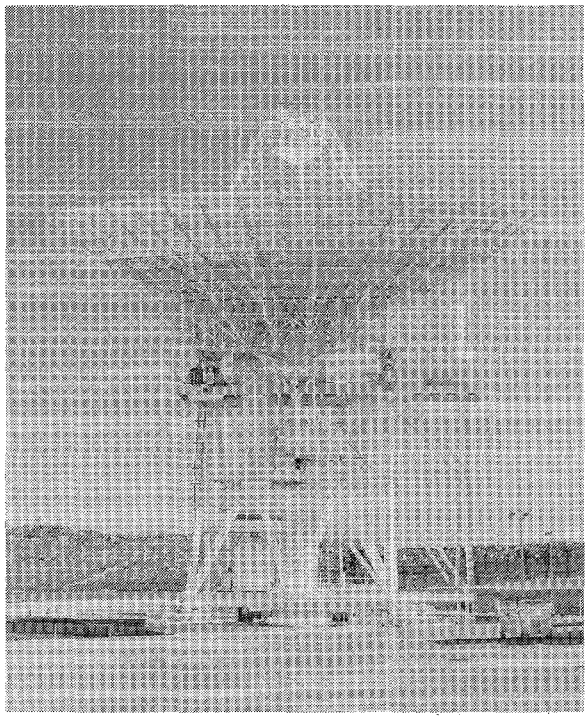

Fig. 1. Front view of the BWG antenna pointed in the zenith direction.

The purpose of this article is to present a methodology for making antenna performance predictions of Cassegrain and BWG antennas. The performance parameters being predicted are antenna area efficiency, corresponding beampeak gains, and operating (system) noise temperatures [1]. *X*-band (8.45 GHz) and *Ka*-band (32 GHz) predicted performance data are presented for the new antenna. The predictions apply only to those equipment configurations and antenna adjustment state that existed during Phase I—a time period allocated for performing initial experimental work between July 1990 and February 1991.

Performance predictions are considered essential for planning, guiding, and judging the final results of a test program of this kind. The performance analyses required are found to assist in identifying critical and/or poorly understood areas that, in turn, suggest fruitful test strategies. Predictions are also found most valuable in re-

Manuscript received May 28, 1991; revised October 11, 1991. The research described in this paper was carried out by the Jet Propulsion Laboratory, California Institute of Technology, under a contract with the National Aeronautics and Space Administration.

The authors are with the Jet Propulsion Laboratory, California Institute of Technology, 4800 Oak Grove Drive, Pasadena, CA 91109.

IEEE Log Number 9107468.

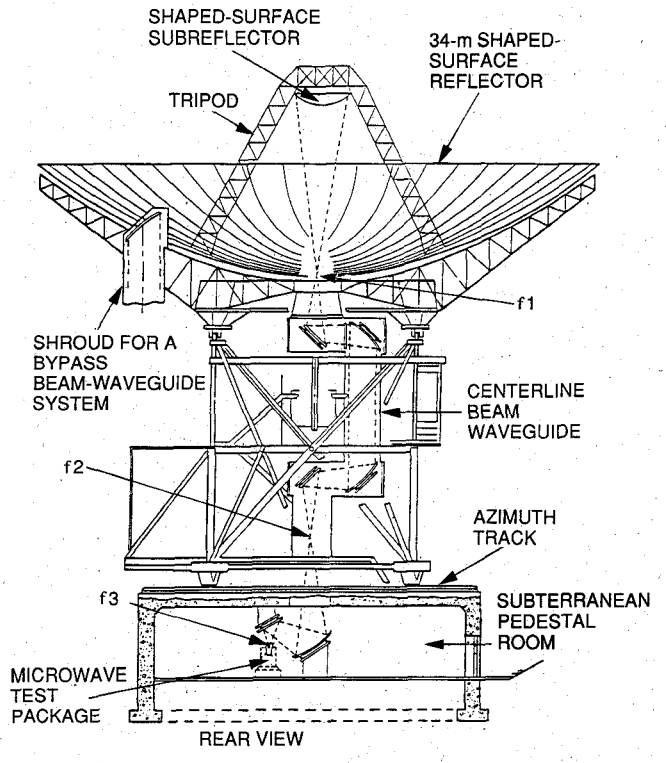

Fig. 2. Rear view of the BWG antenna in the centerline mode, showing focal points.

sponding to unusual events, sometimes requiring important rescheduling. Knowing how close to (or far from) expected performance a system is currently running will determine priorities and influence decision making.

II. BWG Antenna Description and Technical Data

The new DSN antenna provides a centerline beam waveguide subsystem, which places all feed equipment in a subterranean room about 35-m path length distance from the Cassegrain focal point f1. Four major advantages of having equipment in a subterranean room, rather than in a Cassegrain feed housing (cone) are 1) more space is available for a multiplicity of feeds and amplifiers, 2) ease of installations and maintenance of front-end assemblies, 3) elimination of potential degradation caused by noise generated by moisture or rain droplets on the feedhorn window and dichroic plate holes, and 4) the non-tipping environment enables the future use of ultra-low-noise microwave receive assemblies whose horn, waveguide, and amplifiers are all cryogenically-cooled to physical temperatures below 2 K.

The information provided in this section are some of the technical mechanical and microwave data that were used to make predictions. Some of the information were derived from design data while others were based on experimental data.

The new 34-m-diameter BWG antenna is designed with the primary reflector and subreflector as shaped dual-reflectors to provide uniform aperture illumination. The main reflector has an equivalent F/D ratio near 0.32 (where F is the focal length and D is the main reflector diameter). Shaped dual-reflector antennas do not have a geometric optics focal point, but instead have a zone. Thus the F/D ratio cannot be precisely defined. The subreflector diameter is close to 3.430 m. In contrast to quadripod legs used on other DSN antennas to support the subreflector, the new antenna uses tripod legs that have low optical cross-sections (see Fig. 1). The subreflector and all beam-waveguide reflectors are webbed aluminum castings with about 0.125-mm root mean square (RMS) machined finish averaged over the entire reflector surface area. Since most of the microwave beam is carried over a smaller central region where the surface finish of the reflector is typically better, the effective RMS is likely to be better than 0.125-mm RMS. (All RMS numbers quoted are taken normal to the reflecting surface.)

All reflecting surfaces are adequate for high performance at 32 GHz. The main reflector is paneled with doubly-curved solid sheet panels out to a radius of 13 m. Between 13 m and the outer reflector edge at 17 m, perforated panels are used. All main reflector surface panels had about 0.13-mm RMS surface prior to installation.

The perforated panels have 3.2-mm (0.125-inch) hole diameter, 4.8-mm (0.188-inch) hole-to-hole spacing and 1.8-mm (0.070-inch) thickness. Alternate rows of holes are staggered so that adjacent holes form hexagonal hole patterns. Based on approximate formulas given in [2], [3] and the fact that only 42 percent of the total main reflector surface area is perforated, the average effective leakage at 8.45 GHz is predicted to be near -41 dB at 8.45 GHz and -26 dB at 32 GHz. The stated average values are based on taking the average leakage of two orthogonal polarizations at an average incidence angle of 34.2 deg.

For purposes of making predictions, the average gap between panels was estimated to be 3.2 mm (0.125 inch). Assuming that the gap between panels is a parallel plate waveguide, then only the polarization perpendicular to the parallel plate walls transmits through the gap. For a circularly polarized wave, the effective total area of all gaps is one-half the actual area. The ratio of the effective total gap area to the total main reflector surface area for the subject BWG antenna is 0.00185. Estimates of the effective brightness temperatures absorbing the leakage behind the main reflector surface are as follows. For 8.45 GHz, the effective brightness temperatures, for prediction purposes, are estimated to be 267, 205, and 153 K at the 90-, 30-, and 10-deg elevation angles. For 32 GHz the effective brightness temperatures are estimated to be 268, 214, and 166 K at the 90-, 30-, and 10-deg elevation angles. The effective brightness temperatures are based upon approximate numerical integration of leakage over the entire reflector surface. Most of the leakage power is absorbed by an assumed flat desert ground at the various incidence angles considered. The portion of leakage not absorbed by the ground is reflected back to the sky. Values used for calculations were a desert ground relative dielectric constant and conductivity of 3.0 and 0.011

mho/m, respectively, and ground surface physical temperature and relativity humidity of 20°C and 30%, respectively.

After the antenna was constructed, it was found that, instead of the gaps between panels being 3.2 mm (1/8 inch), the gaps were typically larger and about 10% of all gaps between panels were found to have gap widths as large as 4.8 mm (3/16 inch). Thus at 32 GHz, it becomes possible for a TE_{10} mode to propagate through some of the gaps and make measured *Ka*-band values of noise temperatures (due to leakage through gaps) be larger than the predicted values.

Both the solid and perforated panels are made from 6061-T6 aluminum sheets that are painted with a layer of primer and Triangle Co. #6 thermal diffusive white paint. The combined thickness of the primer and white paint is less than 0.05 mm (0.002 inch). Radiometer noise temperature measurements [4] and surface resistivity (R_s) measurements [5] with a cavity-technique provided data used for predicting the noise temperature generated by the Triangle #6 white paint, primer, and aluminum reflector surface materials.

Approximately 1750 panel adjustment holes exist on the main reflector surface. These holes are open for purposes of allowing passage of a tool for making panel adjustments. These holes have a hole diameter of 32 mm (1.25 inch) corresponding to a cutoff frequency for a TE_{11} mode of 5.53 GHz. Account is not taken of the effects of these panel adjust openings because the hole coupling factors are presently unknown and have to be determined in the future by experimental means. It is expected that more coupling occurs at 32 GHz than at 8.45 GHz.

The surrounding tubing (shroud) for the BWG mirror system has a diameter of approximately 2.44 m (8 ft) and is made from ASTM A36 structural hot-rolled steel. The inside surface of the BWG tubing is painted with a layer of primer and Triangle Co. #6 thermal diffusive white paint. Two painted samples of the BWG tube material had a measured effective conductivity (σ/μ_r) of 0.003 E07 mho/m at 8.420 GHz [5] where σ is the actual electrical conductivity and μ_r is the relative permeability. This is a conductivity roughly 1000 times worse than aluminum material, which will cause a loss about 32 times worse. However, little of the beam induces current in the shroud.

III. Methodology

The methodology used for making antenna performance predictions is to account for the effects of all predictable elements that contribute to antenna performance degradations for antenna area efficiencies, corresponding beam peak gain, and noise temperatures. Performance analysis is a combination of analytical model application and estimations based on experience, judgment, and experimental data previously obtained on other DSN antennas.

At f1 (see Fig. 2), the elements taken into account for antenna efficiency and gain are 1) the illumination field pattern losses based on Physical Optics (PO) [6],[1] 2) resistive and spillover losses of main reflector and subreflector, and 3) scattering of the tripod legs and the bypass shroud on the main reflector surface. The elements taken into account for operating noise temperature at f1 include the cosmic background, atmosphere, f1 field spillovers, subreflector and main reflector resistive losses, panel leakage, gap leakage, and the losses due to tripod and bypass scattering. Resistive losses and VSWR associated with the feed-related microwave "plumbing" are included, as discussed later. The additional losses and noise temperature contributions between f1 and f3 include those spillover and resistive losses for the four upper BWG mirrors (two flat and two paraboloidal sections) and the two lower BWG mirrors (an elipsoidal section and flat mirror above the feedhorn in the pedestal room). VSWR losses are also included.

In the following section, comparisons are made between predicted and experimental values at f1 and f3 for *X*- and *Ka*-band frequencies. The experimental data for this article are summaries of test results from companion articles in this issue [8], [9]. The overall test strategy involved first using a *Ku*-band holography test package at f1 to obtain data for optimizing the setting of panels on the main reflector surface (see [10] this issue). Then after the panels were reset, efficiency and noise temperature measurements were made at f1 and f3 at *X*- and *Ka*-band. The technique used for antenna efficiency measurements as well as test results are presented in a separate article in this issue [8]. Descriptions of the *X*- and *Ka*-band test packages used for measurements at f1 and f3, as well as measured noise temperature data, are presented in this issue [9].

Comparisons of test data with the test packages on the ground and at the f1 and f3 locations provided an experimental means for determining degradations caused by different parts of the BWG antenna system. Comparison of experimental data to the predicted values 1) provided confirmation of the predict methodology, 2) helped to identify areas where the antenna did not meet design performance expectations, and 3) helped to isolate contributions that were not yet identified or predicted.

It should be stated that some of the predicted values were based on experimentally determined values. At the start of the BWG antenna project, noise temperature contributions due to BWG mirror spillover were not clearly understood. It was at first assumed that spillover power was eventually absorbed by cold sky or by a cold front-end receiver. However, this assumption turned out to be incorrect and it is more likely that most of the fractional power contained in spillover solid angles are eventually absorbed by an ambient environment (BWG lossy shroud walls and pedestal room). Experimental data obtained more recently was used to update early predictions of

[1]Confirming work was done using Geometrical Theory of Diffraction/Jacobi-Bessel (GTD/JB) scatterings [7]. The agreements were everywhere within 0.09 dB, which is considered excellent.

noise temperature contributions due to BWG mirror spillover. Agreements between predicted and experimental noise temperatures presented in this article are, therefore, somewhat better than agreements previously reported elsewhere [11].

IV. Expected Performance

Itemized accountings for predicted efficiency, gain, and noise temperatures are presented in Tables I–IV for *X*-band, and Tables V–VIII for *Ka*-band. Table IX and X contain summaries of all of the predicted and experimental values data that will be discussed in the following section. The authors have found it helpful to refer to Tables IX and X for making comparisons of results.

Predicted values are given for total contributions at two reference planes. The first and second reference planes are the microwave test-package horn aperture and the HEMT input flange, respectively. Prediction values that are defined at the HEMT input allow direct comparisons to be made with experimentally obtained values. For making antenna efficiency and gain predictions at the HEMT input flange, it is necessary to account for waveguide loss between the horn aperture and HEMT input flange. For noise temperature predictions, it is necessary to account for noise temperature contributions due to waveguide loss, HEMT, and followup receiver. These internal test package loss and noise temperature values used in the predictions are also provided.

A. X-Band Predictions

1. Antenna Area Efficiency and Gain: Tables I and II illustrate applications of the methodology for making antenna efficiency predictions. Accountings are given of the predicted losses for antenna efficiency for *X*-band at f1 and f3, respectively. These predictions are applicable only for a main reflector adjustment or rigging angle at or very close to 45-deg elevation. At f1, the total antenna efficiency and gain for 8.420 GHz at the HEMT input flange are shown to be 0.7887 and 68.51 dBi, respectively. The corresponding predicted total antenna efficiency and gain value at f3 are 0.7445 and 68.26 dBi, respectively.

It should be pointed out that the actual frequency of the R&D tests at *X*-band was 8.450 GHz instead of 8.420 GHz. The 8.420-GHz predictions were based on midband DSN spacecraft-tracking use, and the R&D measurement frequency was determined by an available filter. Therefore, a small correction of 0.031 dB needs to be added to the predicted 8.420-GHz antenna gain for making comparisons to experimental gain values obtained at 8.450 GHz. The corrections needed on antenna efficiency and noise temperature are negligibly small. After application of the 0.031 dB correction to predicted values for 8.420 GHz, shown in Tables I and II, predicted gains of 68.54 and 68.29 dBi for f1 and f3, respectively, are obtained for 8.450 GHz. The measured efficiency and gain at 8.450 GHz is reported to be 0.754 and 68.34 dBi for f1 and 0.724 and 68.17 dBi for f3 [8]. In general, the agreements between predicted and measured *X*-band efficiencies and gains are satisfactory (within 0.20 dB), including both focal points.

2. Operating Noise Temperature: To allow direct comparisons of predicted and measured values of operating noise temperatures, both the predicted and measured values for 8.450 GHz have been normalized to a Goldstone average clear zenith atmosphere of 2.17 K and a waveguide physical temperature of 20°C. Tables 3 and 4, for f1 and f3, respectively, illustrate applications of the methodology for making operating noise temperature predictions. Itemized accountings are given of the predicted contributions to the overall operating noise temperature at 8.420 GHz. The accountings also apply to 8.450 GHz since there are negligible differences between the noise contributions at 8.450 versus 8.420 GHz. Accountings are given for zenith, 30-, and 10-deg elevation angles.

From values given in Table III, the predicted operating noise temperature value of the *X*-band test package on the ground is determined to be 22.7 K, which is in exact agreement with the measured value. The contributors to the on-the-ground operating noise temperature are the cosmic background noise temperature (properly attenuated by the atmospheric and waveguide loss factors), the atmospheric noise temperature (properly attenuated by the waveguide loss factor), and noise temperatures from the waveguide loss, HEMT, and followup receiver.

At f1, the test-package operating noise temperature picks up added reflector associated noise contributions, including rear spillover, resistive loss of the main reflector, panel and gap leakage, resistive loss of the subreflector, and scattering from the tripod and a bypass housing (see Fig. 2). After applying the appropriate waveguide loss factors to individual noise contributions, the predicted zenith operating noise temperature is determined to be 26.0 K as compared to the measured value of 25.9 K [9]. The good agreement of 0.1 K between the predicted and experimental zenith operating noise temperatures at f1 provides confidence in both the Cassegrain prediction methodology as well as the measurement absolute accuracy. Importantly, no significant offset in *X*-band noise (predictions vs. measurements) exists at f1, the familiar Cassegrain focus.

Comparisons of predicted values for a 30-deg elevation angle (in Table III) with experimental tipping curve data [13] shows that the predicted operating noise temperature is about 1.0 K higher than the experimental value. A plausible explanation for this discrepancy is that the new BWG antenna has newly designed slim tripod legs, rather than conventional larger cross-section quadripod legs for subreflector supports used on other DSN antennas. Although experimental data was not obtained for f1 tests down to a 10-deg elevation angle, the tipping curve data indicate that for this BWG antenna, the noise due to tripod-leg scattering remains constant between zenith and 15-deg elevation angles.

It is now of interest to compare predicted and measured differential "f1 minus ground" operating noise tempera-

TABLE I
DSS-13 PHASE I OVERALL GAIN ACCOUNTING X-BAND AT f1

Element		Efficiency	Note
P.O. Computed Subtotal		0.9190 (−0.37 dB)	Includes f1 field: FWD spill 0.987; Rear spill 0.9977; Illum ampl incl; Illum phase incl; Crosspol incl; M ≠ 1 modes incl; Central blockage incl
4 Upper BWG Mirror Spill		—	Not applicable
2 Lower BWG Mirror Spill		—	Not applicable
Main Reflector	I^2R	0.99954	Based on R_s data
	Panel Leakage	0.99992	Calculated (see Section II)
	Gap Leakage	0.9982	Calculated (see Section II)
	RMS	0.9770	Normal 0.45 mm (0.0177 in.)
Subreflector	I^2R	0.99954	Based on R_s data
	RMS	0.9980	Normal 0.125 mm (0.005 in.)
4 BWG Mirror	I^2R	—	Not applicable
	RMS	—	Not applicable
2 BWG Mirror	I^2R	—	Not applicable
	RMS	—	Not applicable
BWG/Cass VSWR		—	Not applicable
Waveguide	I^2R	0.9840	−0.070 dB (measured)
	VSWR	0.99	
Dichroic	I^2R	1.00	None in Phase I
	VSWR	1.00	None in Phase I
Feed Support Blockage		0.918	X-band, tripod, 2.7%, 1.55 factor
Bypass Blockage		0.987	9-ft equivalent diameter
Pointing Squint		—	Negligible loss at rigging angle
BWG Mirror Alignments		—	Not applicable
Total Efficiency		0.7887	−1.03 dB
Overall Gain, dBi		+68.51	+69.54 dBi is 100% at 8420 MHz

TABLE II
DSS-13 PHASE I OVERALL GAIN ACCOUNTING X-BAND AT f3

Element		Efficiency	Note
P.O. Computed Subtotal		0.9099 (−0.41 dB)	Includes f1 field: FWD spill 0.9834; Rear spill 0.9985; Illum ampl incl; Illum phase incl; Crosspol incl; M ≠ 1 modes incl; Central blockage incl
4 Upper BWG Mirror Spill		0.9840	1.60%
2 Lower BWG Mirror Spill		0.9847	1.53%
Main Reflector	I^2R	0.99954	Based on R_s data
	Panel Leakage	0.99992	Calculated (see Section II)
	Gap Leakage	0.9982	Calculated (see Section II)
	RMS	0.9770	Normal 0.45 mm (0.0177 in.)
Subreflector	I^2R	0.99954	Based on R_s data
	RMS	0.9980	Normal 0.125 mm (0.005 in.)
4 BWG Mirror	I^2R	0.99807	Based on R_s data
	RMS	0.9960	Each normal 0.125 mm (0.005 in.)
2 BWG Mirror	I^2R	0.99903	Based on R_s data
	RMS	0.9970	Each normal 0.125 mm (0.005 in.)
BWG/Cass VSWR		0.999	Estimated
Waveguide	I^2R	0.9840	−0.070 dB loss (measured)
	VSWR	0.99	
Dichroic	I^2R	1.00	None in Phase I
	VSWR	1.00	None in Phase I
Feed Support Blockage		0.918	X-band, Tripod, 2.7%, 1.55 factor
Bypass Blockage		0.987	9-ft equivalent diameter
Pointing Squint		0.9954	−0.02-dB scan loss
BWG Mirror Alignments		0.9994	Based on 0.99 at 32 GHz
Total Efficiency		0.7445	−1.281 dB
Overall Gain, dBi		+68.26	+69.54 dBi is 100% at 8420 MHz

TABLE III
DSS-13 PHASE I OVERALL NOISE ACCOUNTING *X*-BAND AT f1

Element	Noise, K 90° El	30° El	10° El	Note
Cosmic Background	2.5	2.5	2.5	Effective blackbody [9]
Atmosphere	2.17	4.34	12.50	Goldstone (average clear) [12]
f1 Fields/Fwd Spill/Gnd	0.	0.	0.16	
4 Upper BWG Mirror Spill	—	—	—	Not applicable
2 Lower BWG Mirror Spill	—	—	—	Not applicable
Main Reflector Rear Spill	0.55	0.38	0.32	0.23%
4 BWG Mirror I^2R	—	—	—	Not applicable
2 BWG Mirror I^2R	—	—	—	Not applicable
Main Reflector I^2R	0.14	0.14	0.14	
Panel Leakage	0.02	0.02	0.01	
Gap Leakage	0.5	0.4	0.3	Calculated (see Section II)
Subreflector I^2R	0.13	0.13	0.13	
Dichroic I^2R	—	—	—	None in Phase I
Scatter	—	—	—	None in Phase I
Tripod Scatter	2.0	3.0	3.5	
Bypass Scatter	0.07	0.42	0.74	
Subtotal	8.08	11.33	20.30	Noise at feed aperture
Waveguide I^2R	4.69	4.69	4.69	−0.070 dB at 20°C
Modify Subtotal[a]	7.95	11.15	19.98	Noise at preamplifier input
Preamplifier	13.0	13.0	13.0	Phase I HEMT
Followup	0.4	0.4	0.4	
Total Noise,[a] K	26.0	29.2	38.1	

[a] The subtotal and total take into account noise contribution attenuations by the waveguide I^2R loss factor, but not by intermediate loss factors associated with reflector and subreflector dissipative losses. However, the error on total noise, caused by neglecting the intermediate loss factors, is less than 0.06 K.

TABLE IV
DSS-13 PHASE I OVERALL NOISE ACCOUNTING *X*-BAND AT f3

Element	Noise, K 90° El	30° El	10° El	Note
Cosmic Background	2.5	2.5	2.5	Effective blackbody [9]
Atmosphere	2.17	4.34	12.50	Goldstone (average clear) [12]
f1 Fields/Fwd Spill/Gnd	0.0	0.0	0.20	
4 Upper BWG Mirror Spill	4.31	4.41	4.50	90% of 1.61% spill is dissipated
2 Lower BWG Mirror Spill	4.59	4.59	4.59	100% of 1.53% spill is dissipated
Main Reflector Rear Spill	0.36	0.25	0.21	0.15%
4 BWG Mirror I^2R	0.572	0.572	0.572	
2 BWG Mirror I^2R	0.272	0.272	0.272	
Main Reflector I^2R	0.136	0.136	0.136	
Panel Leakage	0.02	0.02	0.01	
Gap Leakage	0.5	0.4	0.3	(See Section II)
Subreflector I^2R	0.134	0.134	0.134	
Dichroic I^2R	—	—	—	None in Phase I
Scatter	—	—	—	None in Phase I
Tripod Scatter	2.0	3.0	3.5	
Bypass Scatter	0.07	0.42	0.74	
Subtotal	17.63	21.04	30.16	Noise at feed aperture
Waveguide I^2R	4.69	4.69	4.69	−0.070 dB at 20°C
Modify Subtotal[a]	17.35	20.70	29.68	Noise at preamplifier input
Preamplifier	13.0	13.0	13.0	Phase I HEMT
Followup	0.4	0.4	0.4	
Total Noise,[a] K	35.4	38.8	47.8	

[a] The subtotal and total take into account noise contributions attenuated by the waveguide I^2R loss factor, but not by the intermediate loss factors associated with main reflector, subreflector, BWG I^2R, and BWG spillover losses. The methodology for applying loss factors due to BWG spillover contributions is not clearly understood and is still being studied.

TABLE V
DSS-13 PHASE I OVERALL GAIN ACCOUNTING *Ka*-BAND AT f1

Element		Efficiency	Note
P.O. Computed Subtotal		0.9064 (−0.43 dB)	Includes f1 field: FWD spill 0.9814; Rear spill 0.9995; Illum ampl incl; Illum phase incl; Crosspol incl; M ≠ 1 modes incl; Central blockage incl
4 Upper BWG Mirror Spill		—	Not applicable
2 Lower BWG Mirror Spill		—	Not applicable
Main Reflector	I^2R	0.9991	Based on R_s data
	Panel Leakage	0.9975	Calculated (see Section II)
	Gap Leakage	0.9982	Calculated (see Section II)
	RMS	0.7144	Normal 0.45 mm (0.0177 in.)
Subreflector	I^2R	0.9991	Based on R_s data
	RMS	0.9714	Normal 0.125 mm (0.005 in.)
4 BWG Mirror	I^2R	—	Not applicable
	RMS	—	Not applicable
2 BWG Mirror	I^2R	—	Not applicable
	RMS	—	Not applicable
BWG/Cass VSWR		—	Not applicable
Waveguide	I^2R	0.9397	−0.27 dB loss (measured)
	VSWR	0.99	
Dichroic	I^2R	1.00	None in Phase I
	VSWR	1.00	None in Phase I
Feed Support Blockage		0.918	*Ka*-band, tripod, 2.7%, 1.55 factor
Bypass Blockage		0.987	9-ft equivalent diameter
Pointing Squint		—	Negligible loss at rigging angle
BWG Mirror Alignments		—	Not applicable
Total Efficiency		0.5270	−2.78 dB
Overall Gain, dBi		+78.36	+81.14 dBi is 100% at 32.0 GHz

TABLE VI
DSS-13 PHASE I OVERALL GAIN ACCOUNTING *Ka*-BAND AT f3

Element		Efficiency	Note
P.O. Computed Subtotal		0.8995 (−0.46 dB)	Includes f1 field: FWD spill 0.9853; Rear spill 0.9996; Illum ampl incl; Illum phase incl; Crosspol incl; M ≠ 1 modes incl; Central blockage incl
4 Upper BWG Mirror Spill		0.9888	1.12%
2 Lower BWG Mirror Spill		0.9892	1.08%
Main Reflector	I^2R	0.9991	Based on R_s data
	Panel Leakage	0.9975	Calculated (see Section II)
	Gap Leakage	0.9982	Calculated (see Section II)
	RMS	0.7144	Normal 0.45 mm (0.0177 in.)
Subreflector	I^2R	0.9991	Based on R_s data
	RMS	0.9714	Normal 0.125 mm (0.005 in.)
4 BWG Mirror	I^2R	0.9961	Based on R_s data
	RMS	0.9437	Each normal 0.125 mm (0.005 in.)
2 BWG Mirror	I^2R	0.9982	Based on R_s data
	RMS	0.9575	Each normal 0.125 mm (0.005 in.)
BWG/Cass VSWR		0.999	Estimated
Waveguide	I^2R	0.9397	−0.27-dB loss (measured)
	VSWR	0.99	
Dichroic	I^2R	1.00	None in Phase I
	VSWR	1.00	None in Phase I
Feed Support Blockage		0.918	*Ka*-band, tripod, 2.7%, 1.55 factor
Bypass Blockage		0.987	9-ft equivalent diameter
Pointing Squint		0.9954	−0.02-dB scan loss
BWG Mirror Alignments		0.99	Estimated
Total Efficiency		0.4524	−3.44 dB
Overall Gain, dBi		+77.70	+81.14 is 100% at 32.0 GHz

TABLE VII
DSS-13 PHASE I OVERALL NOISE ACCOUNTING *Ka*-BAND AT f1

Element		Noise, K 90° El	30° El	10° El	Note
Cosmic Background		2.0	2.0	2.0	Effective blackbody [9]
Atmosphere		7.02	14.04	40.43	Goldstone (average clear) [12]
f1 Fields/Fwd Spill/Gnd		0.0	0.0	0.22	
4 Upper BWG Mirror Spill		—	—	—	Not applicable
2 Lower BWG Mirror Spill		—	—	—	Not applicable
Main Reflector Rear Spill		0.13	0.08	0.06	0.05%
4 BWG Mirror I^2R		—	—	—	Not applicable
2 BWG Mirror I^2R		—	—	—	Not applicable
Main Reflector	I^2R	0.27	0.27	0.27	
	Panel Leakage	0.67	0.54	0.42	
	Gap Leakage	0.5	0.4	0.3	Calculated (see Section II)
Subreflector	I^2R	0.26	0.26	0.26	
Dichroic	I^2R	—	—	—	None in Phase I
	Scatter	—	—	—	None in Phase I
Tripod Scatter		2.0	3.0	3.5	
Bypass Scatter		0.07	0.42	0.741	
Subtotal		12.92	21.01	48.20	Noise at feed aperture
Waveguide	I^2R	17.67	17.67	17.67	−0.27 dB at 20°C
Modify Subtotal[a]		12.14	19.74	45.29	Noise at preamplifier input
Preamplifier		56.6	56.6	56.6	Phase I HEMT
Followup		1.8	1.8	1.8	
Total Noise,[a] K		88.2	95.8	121.36	

[a] The subtotal and total take into account noise contributions attenuated by the waveguide I^2R loss factor, but not loss factors associated with main reflector and subreflector dissipative losses. The effect of applying the intermediate loss factors is to reduce the total noise by 0.2 K.

TABLE VIII
DSS-13 PHASE I OVERALL NOISE ACCOUNTING *Ka*-BAND AT f3

Element		Noise, K 90° El	30° El	10° El	Note
Cosmic Background		2.0	2.0	2.0	Effective blackbody [9]
Atmosphere		7.02	14.04	40.43	Goldstone (average clear) [12]
f1 Fields/Fwd Spill/Gnd		0.0	0.0	0.24	
4 Upper BWG Mirror Spill		3.02	3.12	3.21	90% of 1.12% spill is dissipated
2 Lower BWG Mirror Spill		3.24	3.24	3.24	100% of 1.08% spill is dissipated
Main Reflector Rear Spill		0.10	0.06	0.05	0.04%
4 BWG Mirror I^2R		1.11	1.11	1.11	
2 BWG Mirror I^2R		0.53	0.53	0.53	
Main Reflector	I^2R	0.27	0.27	0.27	
	Panel Leakage	0.67	0.54	0.42	
	Gap Leakage	0.5	0.4	0.3	(see Section II)
Subreflector	I^2R	0.26	0.26	0.26	
Dichroic	I^2R	—	—	—	None in Phase I
	Scatter	—	—	—	None in Phase I
Tripod Scatter		2.0	3.0	3.5	
Bypass Scatter		0.07	0.42	0.74	
Subtotal		20.79	28.99	56.30	Noise at feed aperture
Waveguide	I^2R	17.67	17.67	17.67	−0.27 dB at 20°C
Modify Subtotal[a]		19.54	27.24	52.91	Noise at preamplifier input
Preamplifier		56.6	56.6	56.6	Phase I HEMT
Followup		1.8	1.8	1.8	
Total Noise,[a] K		95.6	103.3	129.0	

[a] The subtotal and total take into account the noise contribution attenuation the waveguide I^2R, but not intermediate loss factors associated with main reflector, subreflector, BWG I^2R and spillover losses. The methodology for applying loss factors due to BWG spillover contributions is not clearly understood and is still being studied.

TABLE IX
COMPARISON OF PREDICTED AND MEASURED RF PERFORMANCE VALUES FOR TEST PACKAGE IN VARIOUS SYSTEM CONFIGURATIONS

Frequency, GHz	System Configuration	45 deg El Efficiency		45 deg El Gain, dBi		Zenith Operating Noise Temp, K		
		Predict	Measured	Predict	Measured	Predict	Measured	Measured-Predict
8.450	TP[a] on ground	N/A	N/A	N/A	N/A	22.7[b]	22.7	0.0
8.450	TP at f1	0.789	0.754	68.54	68.34	26.0	25.9	−0.1
8.450	TP at f3	0.745	0.724	68.29	68.17	35.4	34.8	−0.6
32.0	TP on ground	N/A	N/A	N/A	N/A	84.5[b]	84.7	0.2
32.0	TP at f1	0.527	0.523	78.36	78.33	88.2	91.8	3.6
32.0	TP at f3	0.452	0.449	77.70	77.66	95.6	98.6	3.0

[a] TP denotes test package [9].
[b] Contributions from cosmic, atmosphere, waveguide I^2R, preamplifier, followup as adjusted with applicable atmosphere and waveguide loss factors.
N/A = Not applicable. The test package on ground does not provide reflector-antenna-like (useable) levels of gain and is therefore not predicted, nor measured.

TABLE X
DIFFERENTIAL ZENITH OPERATING NOISE TEMPERATURES (FROM VALUES GIVEN IN TABLE IX)

Frequency, GHz	System Configurations	Differential Values		
		Predict, K	Measured, K	Measured-Pred, K
8.450	f1–ground	3.3	3.2	−0.1
8.450	f3–f1	9.4	8.9	−0.5
32.0	f1–ground	3.7	7.1	3.4
32.0	f3–f1	7.4	6.8	−0.6

tures (see Table X). This differential value provides information concerning only the Cassegrain antenna portion of the overall antenna. The predicted and measured "f1 minus ground" operating noise temperatures are, respectively, 3.3 K and 3.2 K. The agreement to within 0.1 K provides a comforting closure for the Cassegrain (f1) focus.

At f3, the test package picks up additional noise contributions due to BWG mirror spillover and the resistive losses of the BWG mirrors. After applying loss factors as appropriate for the individual noise contributors, the predicted operating noise temperature at f3 is 35.4 K as compared to an experimental value of 34.8 K (as measured after realignment of certain BWG mirrors on December 18, 1990). The 0.6-K disagreement (35.4-K prediction, 34.8-K measured) at f3 might be due to the prediction of slightly more spillover than actually exists for the pedestal room mirrors.

The differential "f3 minus f1" operating noise temperature value gives information concerning contributions due to only the BWG portion of the antenna system. From the above, the "f3 minus f1" operating noise temperatures are, respectively, 9.4 K (prediction) and 8.9 K (measured) at *X*-band. From prediction values given in Table IV, it can be seen that 4.3 K of this 9.4-K increase is due to spillover past gaps (~50 to 150 mm) between mirror and shroud walls. Also, an additional 4.6 K comes from spillover past the edges of two unshrouded BWG mirrors in the pedestal room. Presumably, these spillover noise temperature contributions might be reduced in the future, to the extent that we learn how to direct a substantial fraction of the spills to the cold sky.

Thus, as implemented, the DSS-13 BWG at *X*-band was predicted to cause a loss of 0.25 dB in gain and to increase noise 9.4 K (26.0-K f1 to 35.4-K f3). The measurements proved a 0.17-dB loss in gain and 8.9-K increase (25.9-K f1 to 34.8-K f3) in noise. The discrepancy between measured and predicted *X*-band noise contributions of the beam-waveguide portion is 0.5 K (9.4-K predicted, 8.9-K measured).

B. Ka-Band Predictions

1. Antenna Area Efficiency and Gain: Tables V and VI, for f1 and f3, respectively, present accountings of losses for antenna efficiency and gain at *Ka*-band (32 GHz). These predictions are applicable only for a main reflector adjustment or rigging angle near 45-deg elevation. The predicted f1 total efficiency and overall gain at the HEMT input are shown to be 0.527 and 78.36 dBi, respectively. The corresponding measured efficiency and gain are reported to be 0.523 and 78.33 dBi [8]. At f3,

the predicted total antenna efficiency and overall gain at 32 GHz are, respectively, 0.452 and 77.70 dBi, as compared to the measured efficiency and gain values of 0.449 and 77.66 dBi [8]. In general, the agreements between predicted and measured *Ka*-band efficiencies and gains are completely satisfying, even uncommonly good.

2. *Operating Noise Temperature:* To allow direct comparisons of predicted and measured values of operating noise temperatures, both the predicted and measured values for 32.0 GHz have been normalized to a Goldstone average clear zenith atmosphere of 7.02 K and a waveguide physical temperature of 20°C. Tables VII and VIII, for f1 and f3, respectively, give itemized accountings of the predicted contributions to the overall operating noise temperature at 32.0 GHz. Accountings are given for zenith, 30-, and 10-deg elevation angles.

From values given in Table VII, a predicted operating noise temperature value of the *Ka*-band test package on the ground is determined to be 84.5 K, which is in close agreement with the measured value of 84.7 K [9]. The predicted value is obtained by summing up contributions from the cosmic background noise temperature (properly attenuated by the atmospheric and waveguide loss factors), the atmospheric noise temperature (properly attenuated by the waveguide loss factor), and noise temperatures from the waveguide loss, HEMT, and followup receiver.

At f1, the *Ka*-band test package operating noise temperature picks up added noise from reflector contributions, including rear spillover, resistive loss of the main reflector, panel and gap leakage, resistive loss of the subreflector, and scattering from the tripod and a bypass housing (see Fig. 2). After applying the appropriate waveguide loss factors to individual noise contributions, the predicted operating noise temperature is determined to be 88.2 K, as compared to the measured value of 91.8 K [9]. The measured value is 3.6 K higher than the predicted value. Possible explanations for this higher value are 1) more effect at *Ka*-band from the larger than expected gaps (see Section II) between many panels on the main reflector surface, 2) more noise pickup than predicted due to scattering from the tripod and bypass housing at *Ka*-band, 3) the increased leakage (at *Ka*-band) through 4.8-mm (3/16-inch) diameter holes of a temporary perforated *X*-band screen covering the bypass opening on the main reflector surface, 4) surface roughness (rms) scattering coupling hot sources to the horn, and 5) *Ka*-band leakage through panel adjustment holes (see Section II).

It is now of interest and instructive to compare predicted and measured differential values (see Table X). The "f1 minus ground" operating noise temperature value provides information concerning only the Cassegrain antenna portion of the overall antenna. Table X shows that the predicted and measured "f1 minus ground" values differ by 3.4 K. This value results from (see Table IX) the measured operating noise temperature at f1 being 3.6-K higher than the predicted value, while the measured and predicted operating noise temperature for the test package on the ground agrees to within 0.2 K. Possible causes of the higher than expected measured f1 value have already been given above.

At f3, the test package picks up additional noise contributions due to BWG mirror spillover and the resistive losses of the BWG mirrors. After applying loss factors as appropriate for the individual noise contributors, the predicted operating system at f3 is shown in Table IX to be 95.6 K, as compared to an experimental value of 98.6 K (as measured after realignment of certain BWG mirrors on December 18, 1990). Most of the 3.0-K disagreement (95.6-K prediction, 98.6-K measured) at f3 is due to the measured value at f1 also being higher than the predicted value by approximately the same amount. The same sources that contribute to the measured operating noise temperature being higher at f1 also would cause the measured operating noise temperature at f3 to be higher by the same amount (except for slight adjustment needed to be made to account for the BWG loss factor).

The differential "f3 minus f1" operating noise temperature value gives information concerning noise contributions due to only the BWG portion of the antenna system. As shown in Table X, the "f3 minus f1" operating noise temperatures are, respectively, 7.4 K (prediction) and 6.8 K (measured). The discrepancy between the predicted and measured "f3 minus f1" value is 0.6 K at *Ka*-band.

Thus, as implemented, the DSS-13 BWG at *Ka*-band was predicted to lose 0.66 dB in gain and to increase 7.4 K in noise (88.2-K f1 to 95.6-K f3). The measurements showed a loss of 0.67 dB in gain and increased noise of 6.8 K (91.8-K f1 to 98.6-K f3). The discrepancy between measured and predicted *Ka*-band noise contributions of the beam-waveguide portion is only 0.6 K (7.4-K predicted, 6.8-K measured).

V. Conclusion

A methodology has been presented for making predictions of a microwave BWG antenna performance. Comparisons of predicted and experimental values have been provided for the normal Cassegrain and centerline BWG modes of the DSS 13 34-m R&D antenna for *X*- and *Ka*-bands. Table IX provides a summary of all predicted and experimentally obtained values for efficiency, gain, and operating noise temperatures for the different test package locations. Table X provides a similar reference table for differential operating noise temperatures. Tables IX and X show that the predictions and experimental values agree reasonably well for gain and efficiency, but not for all noise temperatures. The causes of differences between predicted and measured noise temperatures are currently being investigated.

The usefulness of predictions has been demonstrated. Disagreements between theory and experiment often point out areas where errors might have been made either in theory or experiment. Contributions not taken into account by theory are sometimes uncovered, and excellent (sometimes crucial) guidance is given to the experimenters. One example of crucial guidance involves tightly orchestrated scheduling decisions, as determined by RF performance levels already achieved (or not). Future projects of this kind should clearly invest in the effort required to produce excellent RF predictions.

The authors acknowledge the remarkable radiometric accuracy and stability achieved in this work. Truly superb measurements resulted, and good conclusions have been reached. Without careful predictions, one merely reports measurements.

Acknowledgment

The experimental antenna efficiency and gain values for this article were obtained by a coordinated team and summarized by S. D. Slobin of the Jet Propulsion Laboratory in Pasadena, California.

References

[1] "IRE standards on electron tubes: Definitions of terms, 1962 (62 IRE 7.52)," in *Proc. IEEE*, vol. 51, p. 434, Mar. 1963.

[2] T. Y. Otoshi, "RF properties of the 64-m diameter antenna mesh material as a function of frequency," in *The Deep Space Network Progress Report for September and October 1972*, Technical Report 32-1526, vol. XII, pp. 26–31, Jet Propulsion Laboratory, Pasadena, CA, Dec. 15, 1972.

[3] ——, "Precision reflectivity loss measurements of perforated-plate mesh materials by a waveguide technique," *IEEE Trans. Instrum. Meas*, Special Issue, vol. IM-21, no. 4, pp. 451–457, Nov. 1972.

[4] T. Y. Otoshi and M. M. Franco, "Radiometric tests on wet and dry antenna reflector surface panels," in *The Telecommunications and Data Acquisition Progress Report 42-100*, pp. 111–130, Jet Propulsion Laboratory, Pasadena, CA, Feb. 15, 1990.

[5] T. Y. Otoshi, M. M. Franco, and H. F. Reilly, Jr., "Measurements on the beam waveguide antenna shroud samples and other antenna reflector surface materials," *TDA Progress Report 42-108*, Jet Propulsion Laboratory, Pasadena, CA, Feb. 15, 1992.

[6] R. G. Kouyoumjain and P. H. Pathak, "A uniform geometrical theory of diffraction for an edge in a perfectly conducting surface," *Proc. IEEE*, vol. 62, pp. 1448–1461, Nov. 1974.

[7] V. Galindo-Israel and R. Mittra, "A new series representation for the radiation integral with application to reflector antennas," *IEEE Trans. Antennas Propagat.*, vol. 25, pp. 631–641, Sept. 1977.

[8] S. D. Slobin, T. Y. Otoshi, M. J. Britcliffe, L. S. Alvarez, S. R. Stewart, and M. M. Franco, "Efficiency measurement techniques for calibration of a prototype 34-m-diameter beam-waveguide antenna at 8.45 and 32 GHz," *IEEE Trans. Microwave Theory Tech.*, vol. 40, no. 6, June 1992.

[9] T. Y. Otoshi, S. R. Stewart, and M. M. Franco, "Portable microwave test packages for beam-waveguide antenna performance evaluations," *IEEE Trans. Microwave Theory Tech.*, vol. 40, no. 6, June 1992.

[10] D. J. Rochblatt and B. L. Seidel, "Microwave Antenna Holography," *IEEE Trans. Microwave Theory Tech.*, vol. 40, no. 6, June 1992.

[11] D. A. Bathker, W. Veruttipong, P. W. Cramer, Jr., and T. Y. Otoshi, Ch. 3 in "DSS-13 beam waveguide antenna project: Phase 1 final report," *JPL Document D-8451* (internal document), Jet Propulsion Laboratory, Pasadena, CA, May 15, 1991.

[12] S. D. Slobin, "Atmospheric and environmental effects," Module TCI-40; Rev. C, in the *DSN/Flight Project Interface Design Document 810-5; Rev. D*, (internal document), Jet Propulsion Laboratory, Pasadena, CA, 1991.

[13] T. Y. Otoshi, S. R. Stewart, and M. M. Franco, "A portable *X*-band front-end test package for beam-waveguide antenna performance evaluation part II: Tests on the antenna," *TDA Progress Report 42-105*, Jet Propulsion Laboratory, Pasadena, CA, pp. 54–68, May 15, 1991.

Dan A. Bathker (S'59–M'62–SM'75) was born in Minnesota in 1938. He received the B.S. degree in electronic engineering from California State Polytechnic College, San Luis Obispo, in 1961.

While a student, he became interested in the (then) new wide-band antennas and completed an investigation and construction/test project of a VHF log periodic antenna. Since joining the Jet Propulsion Laboratory Telecommunications Division in 1963, he has enjoyed furthering the microwave antenna capabilities of the NASA/JPL Deep Space Network. This work has included ultra-high CW power transmission with low-noise reception, high accuracy radio flux calibrations and reliable antenna standards, high performance multifeed and simultaneous multiband feeds, correlation of microwave with large reflector structural performance, and planning and designing new deep space communications capabilities. He is Supervisor of the Antenna and Microwave Development Group at JPL and has developed a strong interest in the history and development of all forms of EM communications. He will recognize his 40th year as a licensed radio amateur in 1993.

Mr. Bathker is a member of PG-AP and PG-MTT. He received a NASA exceptional engineering achievement medal in 1984 "for sustained contributions and leadership in application of high performance ground microwave technology resulting in many-fold increases in data return from deep space missions."

Watt Veruttipong (S'77–M'78–SM'90) received B.S. degree in electrical engineering from Chulalongkorn University, Bangkok, Thailand, in 1971, the M.S. and Ph.D. degrees in electrical engineering from The Ohio State University, Columbus, in 1979 and 1982, respectively.

He joined JPL, California Institute of Technology in 1984 as a full time Member of Technical Staff. At JPL, he performs research and development in the areas of applied electromagnetic theory, antennas, and microwaves. This work has resulted in a number of publications concerning the geometrical theory of diffraction, beam-waveguide design and analysis, dual shaped reflector design and analysis, distortion-compensating surface technology, and other antenna research and application areas. He is the Chief Design Engineer for conceptually new beam-waveguide antennas being investigated, tested, and constructed for several future large ground stations in the NASA deep space network. He received the graduate research associate award for the outstanding dissertation of 1982 from the ElectroScience Laboratory, Ohio State University.

Tom Y. Otoshi (S'53–M'56–SM'74), for a photograph and biography, see this issue, p. 1292.

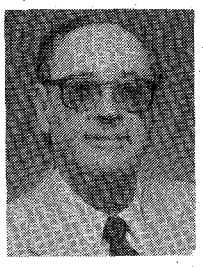

Paul Wm. Cramer was born in Cincinnati, OH, on February 28, 1932. He received the B.S.E.E. degree from the California Institute of Technology in 1955 and the M.S.E.E. degree from the University of California at Los Angeles in 1972.

From 1954 to 1956, he was an Engineer at Aerojet General, Azusa, CA where he was involved in infra-red missile guidance systems. From 1956 to 1982, he was employed at the Jet Propulsion Laboratory, Pasadena, CA, starting as a research engineer in the antenna group working on monopulse tracking antennas. In 1961, he was promoted to Supervisor of the Spacecraft Antenna Group which was responsible for the Ranger and Mariner series spacecraft antennas and associated antenna research activities. In 1969, he became a Member of the Technical Staff working on advanced spacecraft antenna research programs such as communication satellites, land mobile satellite service and large space erectable antennas. From 1982 to 1988, he was employed by the Communication Satellite Corporation as Principal Antenna Engineer in their satellite program monitoring and consulting office and was involved in the SBS, Geostar, Inmarsat, Intelsat and Mexico's Morelos satellite programs. In 1988, he returned to the Jet Propulsion Laboratory as a Member of the Technical Staff in the Ground Antenna and Facilities Engineering Section where his primary activity has been in the use of array feeds to compensate for gravitational distortions of large antenna structures.

Mr. Cramer was awarded a U.S. Patent for a Beam Forming Network on March 5, 1985.